Research Square

Preprints are preliminary reports that have not undergone peer review.
They should not be considered conclusive, used to inform clinical practice,
or referenced by the media as validated information.

Cerium oxide modified biochar as an adsorbent for efficient phosphorus recovery

Lang Wang
Jiangsu University of Technology
Zhiyi Sun
Changzhou Institute of Technology
Haitao Sha
101232727@czu.cn

Changzhou Institute of Technology
Hui Wang
Jiangsu University of Technology

Research Article

Keywords: Biochar, Cerium, Adsorption, Phosphorus, Kinetics

Posted Date: August 10th, 2026

DOI: https://doi.org/10.21203/rs.3.rs-10201538/v1

License: This work is licensed under a Creative Commons Attribution 4.0 International License.
Read Full License

Additional Declarations: No competing interests reported.

Cerium oxide modified biochar as an adsorbent for efficient phosphorus recovery

Lang Wang[a], Zhiyi Sun[b], Haitao Sha[b*], Hui Wang[a*]

[a]*School of Resources and Environmental Engineering, Jiangsu University of Technology, Changzhou 213001, China*

[b]*Research Center of Secondary Resources and Environment, School of Chemical Engineering and Materials, Changzhou Institute of Technology, Changzhou 213032, China*

*Corresponding author.

E-mail address: 101232727@czu.cn, 1316608390@qq.com

ABSTRACT

Excessive phosphorus in water bodies is a key trigger for eutrophication, leading to algal blooms and explosive proliferation of aquatic plants. These blooms disrupt the structure and function of aquatic ecosystems, and produce potent hepatotoxins or neurotoxins, threatening drinking water safety and public health. This study prepared cerium oxide-modified biochar (Ce-BC) using bamboo as a raw material via a cerium oxide hydrothermal method and systematically evaluated its adsorption performance for phosphorus in water. The material was characterized using scanning electron microscopy (SEM), Fourier transform infrared spectroscopy (FTIR), N_2 adsorption-desorption, X-ray diffraction (XRD), and thermogravimetric analysis (TG). The FTIR analysis indicated the abundant presence of hydroxyl groups on the Ce-BC. The point of zero charge of Ce-BC was approximately 6.39. Adsorption experiments demonstrated that compared to BC, Ce-BC exhibited substantially improved adsorption capacity and rate for phosphorus. The adsorption kinetics followed the pseudo-second-order model, and the isotherm data were best fitted by the Dubinin-Radushkevich model, indicating an endothermic and spontaneous chemisorption process.

Key words: Biochar, Cerium, Adsorption, Phosphorus, Kinetics.

1. Introduction

In global ecological environment governance, the loss of non-point source phosphorus from agriculture and discharge of industrial phosphorus-containing wastewater leading to water eutrophication represent significant environmental issues that threatens the stability of aquatic ecosystems and regional ecological security. Phosphorus can persist in water bodies for extended periods and bioaccumulate through the food chain, causing chronic and genetic toxicity to aquatic organisms, which gradually become a class of persistent and widespread pollutants in the environmental field(Durairaj et al. 2024). The sources of these pollutants are closely linked to human activities. According to the previous studies, industrial discharge is a major source of phosphorus pollution in water bodies, which indicates that the total phosphorus concentration in some industrial wastewaters can exceed 100 mg/L(Li et al. 2023, Ryu et al. 2022). These pollutants are highly toxic and stable, making them difficult to remove completely by conventional biological treatments, leading to the discharge of phosphorus into natural water bodies and posing ecological risks(Gray et al. 2020). The exceed phosphorus in water body not only inhibit cholinesterase activity in aquatic organisms and interfere with photosynthesis but can also enter the human body through drinking water or aquatic products, threatening neurological, endocrine, and reproductive health(Sharma et al. 2019). Furthermore, the released inorganic phosphorus can exacerbate water eutrophication, inducing algal blooms and red tides, and the following algal toxin generated from the cyanobacteria can induce the death of aquatic organisms(Brooker et al. 2018, Paerl et al. 2018). Therefore, it is crucial to develop technologies which was capable to both efficiently decrease phosphorus and recover phosphorus resources for promoting phosphorus recycling and ensuring water security.

Current phosphorus removal technologies, such as chemical precipitation, adsorption, advanced oxidation processes, and biological methods, each have limitations. Chemical precipitation is simple to operate but consumes large amounts of chemicals would produce significant sludge and cause the risk of secondary pollution. Advanced oxidation technologies just only can effectively degrade organic phosphorus, which was week to be applied in catalyst separation where the poor recyclability hinder their practical application(Abdullah et al. 2022, Imran and Ahmed 2025, Jatoi et al. 2021, Ponnuchamy et al. 2021, Tony and Mansour 2019). Biological methods are environmentally compatible, but microbial activity is easily influenced by environmental factors, resulting in low treatment efficiency

and insufficient stability(Zhao et al. 2021). These methods struggle to simultaneously achieve efficient organophosphorus removal and phosphorus resource recovery. Meanwhile, the adsorption has attracted more and more attention due to its low energy consumption, cost efficiency and flexibility in design and operation, but the choose of optimal adsorbent was still considered.

Addressing these challenges, the development of novel adsorbent materials represents a key direction for overcoming current technological bottlenecks. Biochar, derived from biomass pyrolysis, offers advantages such as wide raw material availability, high specific surface area, and abundant surface functional groups, demonstrating great potential in pollutant adsorption and catalytic degradation(Ashiq et al. 2019, Kumar et al. 2024, Liang et al. 2021, Lyu et al. 2020, Zhou et al. 2021). Modification with transition metals can further regulate its surface chemical properties, enhancing its adsorption capacity and selectivity for phosphorus. Metal ions coordinate with oxygen-containing functional groups on the biochar surface, forming stable metal-organic complexes or nanoparticles, which increase active sites and improve the material's ability to capture and immobilize phosphorus(Komnitsas et al. 2017). Meanwhile, the previous literature stated the hydrous cerium oxide nanoparticle can successfully remove the As(III) and As (II), which stated the excellent performance of cerium oxide due to the formed hydroxyl groups on the surface(Li et al. 2012).

This study employed a hydrothermal method to prepare cerium dioxide-modified bamboo biochar (Ce-BC), which focuseed on the interaction between cerium dioxide and the biochar matrix, regulated the surface chemistry and systematically evaluated its phosphorus adsorption performance. The character of Ce-BC was examined by Scanning Electron Microscope (SEM), Fourier Transform spectra (FTIR), Brunauer Emmett Teller (BET), X-ray diffraction spectra (XRD) and Thermo-gravimetric Analysis (TG). The effects of dosage, initial concentration, and time on the adsorption process were investigated in this work. To better elucidate the adsorption mechanisms, it was elucidated through isotherm and kinetic models, providing a new approach for developing efficient phosphorus recovery materials.

2. Materials and methods

2.1. Materials

Potassium dihydrogen phosphate, sodium hydroxide, hydrochloric acid, sulfuric acid, ascorbic

acid, ammonium molybdate, potassium antimonyl tartrate, cerium nitrate, ethanol, and urea were purchased from Sigma-Aldrich (Shanghai, China), all with purities exceeding 99%. All solutions were prepared using Milli-Q water.

2.2. Preparation of Ce-BC

Bamboo skin was pulverized into fine powder using a high-speed grinder. The bamboo powder was pyrolyzed under limited oxygen conditions in a muffle furnace. The pyrolysis program was set as follows: heat from 20°C to 400°C during 2 hours and hold at 400°C for 3 hours. The obtained product was collected and sieved through a 100-mesh sieve to obtain bulk bamboo biochar (BC). The BC was then placed in deionized water and ultrasonicated at 30°C for 30 min to improve particle dispersion and prevent agglomeration(Khayyam Nekouei et al. 2024, Marien et al. 2019). It was dried at 373 K for 24 hours, stored in a desiccator, and used as the adsorbent in subsequent experiments.

The BC was subsequently pretreated by soaking in a 65% nitric acid solution with stirring at room temperature for 24 hours to increase the content of carboxyl or hydroxyl groups on the carbon surface, facilitating subsequent cerium ion attachment. The acid-treated particles were then separated by centrifugation, washed with deionized water until the supernatant pH reached 7, and dried overnight in an oven. Afterwards, cerium nitrate was dissolved in ethanol to obtain a 0.02 M ethanol-cerium solution. Then, 0.25 g of BC and 0.75 g of urea were added to 25 mL of this solution. After stirring for at least 30 minutes, the suspension was transferred into a 50 mL Teflon-lined autoclave and heated at 180°C for 3 hours to form cerium oxide-modified bamboo biochar. The last particles were washed with deionized water, dried in an oven at 100°C for 24 hours, and finally ground using a mortar and pestle to obtain the powder(Abdo et al. 2023, Amalina et al. 2022, An et al. 2024, Bhardwaj and Singh 2023, Fionah et al. 2024, Mankomal and Kaur 2022, Pandiarajan et al. 2025, Zhao et al. 2020). The powder was passed through a 100-mesh sieve, and the final product was designated as cerium-modified bamboo biochar (Ce-BC).

2.3. Characterization

The surface morphology changes of bamboo biochar (BC) and cerium-modified bamboo biochar (Ce-BC) before and after modification and adsorption experiments were observed using scanning electron microscopy (SEM) at different magnifications. Qualitative analysis of the evolution of surface

chemical functional groups was performed using Fourier transform infrared spectroscopy (FTIR) in the wavelength range of 400-4000 cm^{-1}. Structural changes in the biochar before and after modification and adsorption tests were examined using an X-ray diffractometer (XRD, PW1140/90, Netherlands) with a Cu Kα radiation source over a 2θ range of 5° to 80°. The Brunauer-Emmett-Teller (BET) specific surface area and pore size distribution were determined using N_2 adsorption-desorption isotherms at 77 K measured with a Micromeritics ASAP 2020 static volumetric analyzer. Additionally, thermogravimetric analysis (TA) was conducted under an air atmosphere at a constant heating rate to quantify the thermal stability and weight loss behavior of the samples.

2.4. Adsorption experiments

The factors influencing phosphorus adsorption include reaction time, adsorbent dosage, initial adsorbate concentration, and temperature. To systematically study the effects of these parameters, batch experiments were designed as follows: The pH effect was investigated by adjusting 50 mg/L phosphorus solutions containing limited adsorbent with pH ranging from 2-10 using dilute HCl or NaOH, followed by shaking in a constant temperature shaker at 25°C for 4 hours before sampling and analysis. To determine the effect of contact time, 50 mg/L potassium dihydrogen phosphate solutions were mixed with adsorbent in 100 mL conical flasks at the optimal pH and shaken at 150 rpm and 25°C. Samples were taken at 0, 30, 60, 120, 240, 360, and 480 min, filtered through a 0.45 μm membrane, and the phosphorus concentration was determined by the ammonium molybdate spectrophotometric method. To assess the effects of temperature and adsorbent dosage under optimal conditions, 50 mg/L phosphorus solutions were prepared with varying adsorbent dosage where the adsorbent dosage ranged from 0.2 to 5 g/L, and shaken at 150 rpm for 4 hours at 298, 308, and 318 K, respectively. After filtration (0.45 μm), phosphorus concentration was measured. To study the effect of initial adsorbate concentration, 200 mg/L phosphorus stock solution was diluted to concentrations of 5, 10, 20, 50, 80, 100, and 200 mg/L. 50 mL of each concentration was placed in conical flasks, 0.1 g adsorbent was added to each, and after reaction under identical shaking conditions for 4 hours, samples were filtered and analyzed. All adsorption experiments were performed in triplicate or more.

The concentration of phosphorous concentration was determined using the ammonium molybdate spectrophotometric method(Zhang et al. 2022). The removal efficiency and adsorption capacity (q_e)

were calculated by following equations:

$$\text{Removal}\ (\%) = \frac{C_0 - C_e}{C_0} \times 100 \quad (1)$$

$$q_e = \frac{(C_0 - C_e)V}{M} \quad (2)$$

where C_0 (mg/L) and C_e (mg/L) are initial and equilibrium phosphorus concentrations, V (mL) is the volume of the solution and M (g) is the mass of the adsorbent.

2.5. Recyclability and regeneration

The recyclability and regeneration of Ce-BC were conducted over eight consecutive and repetitive adsorption-desorption cycles. The sodium hydroxide (0.1 M) was mixed with exhausted Ce-BC and shaken for 120 min at room temperature. Then, refreshed Ce-BC was retrieved and washed with DI water for the following cycles.

3. Results and discussion

3.1. Characterization of adsorbents

SEM images of the two adsorbents were shown in Figure 1. Images of BC and Ce-BC at 5μm and 50μm were selected for comparison. The SEM of BC at 5μm showed obviously distributed surface pores, where these porous structures can promote the accumulation of organic matter and provide physical protection, reducing its decomposition(Sathishkumar et al. 2020). The surface of Ce-BC at 5μm is uniformly covered with numerous fine, granular substances. Compared to BC, these newly formed nanoparticles confirm the successful anchoring of cerium oxide nanoparticles onto the biochar surface. Similar granular modifications were observed on the surface of Ce-BC at 50μm, confirming the generality of the cerium loading process. In addition, Ce-BC showed more fragmented than BC, whether at 5 μm, or at 5 μm, indicating that Ce-BC owned more contact area with adsorbent. Furthermore, gel-like substances present on the BC surface disappeared after modification, indicating that the loading process may have removed some surface organic matter.

FTIR analysis further confirmed that cerium loading involved significant chemical interaction with oxygen-containing functional groups on the biochar surface, rather than mere physical attachment. As shown in Figure 2, the pristine biochar exhibited abundant surface oxygen-containing functional groups, which form the basis for its good hydrophilicity and metal ion complexation capacity. The peaks of 2968 cm^{-1} was related to asymmetric and symmetric aliphatic C-H stretching(Janarthanan et

196 al. 2021), and the peak at 1588 cm^{-1} corresponded to the stretching of aromatic C=C. The observed
197 peak at 1190 cm^{-1} may be due to the stretching of C-O-C bonds in cellulose and
198 hemicellulose(Pasieczna-Patkowska et al. 2025) In Figure 2b, the peaks at 2977 cm^{-1} and 1525 cm^{-1}
199 were similar to the peaks in BC, which were attributed to asymmetric and symmetric aliphatic C-H
200 stretching and stretching of aromatic C=C, respectively. However, the peak at 1374 cm^{-1} corresponded
201 to the planar bending deformation of the -OH group in phenols or $-CH_3$ in aliphatic compounds, and
202 the peak at 1066 cm^{-1} belong to the symmetric and asymmetric stretching vibrations of the O-C=O
203 group in organic components(Ksapabutr et al. 2004).
204 As shown in Figure 3, the BET surface area and pore size of BC and Ce-BC were investigated
205 via N_2 adsorption-desorption measurements. The results exhibited that the adsorption/desorption
206 isotherm was regarded as type-IV isotherm characteristics accompanied by an H4-type hysteresis
207 loop(Mel'gunov 2022, Sing and Williams 2004). This result clearly indicated that the material
208 possesses a typical mesoporous structure, often associated with slit-shaped pores composed of plate-
209 like particles. This aligned well with the loose, layered stacking morphology observed in Figure 1 of
210 BC. In Figure 3b, it showed the isotherm of the cerium-modified composite. Compared to BC, the
211 entire adsorption-desorption curve of Ce-BC was shifted upward, directly and qualitatively indicating
212 a significant reduction in nitrogen adsorption capacity. This leads to the following key conclusions:
213 The increase in adsorption capacity corresponds directly to an increase in the total specific surface area
214 and total pore volume of the material (as listed in Table S1 of the SI). In addition, the isotherm of Ce-
215 BC still maintains type-IV characteristics and an H4-type hysteresis loop, indicating that the overall
216 mesoporous skeleton structure of the material was preserved.
217 The TG curves for BC and Ce-BC were shown in Figure 4. It was observed that the inflection
218 point of change of temperature was nearly 400 ℃, that the weight of BC decreased sharply above
219 400 ℃. Combined to the production temperature of BC, the weight loss of BC above 400 ℃ in Figure
220 4a may be due to the decrease of the residual organic matters in BC(Sha et al. 2024). The TG curve of
221 Ce-BC decreased gradually, on the one hand the residual organic matters in Ce-BC also reduced with
222 the increase of temperature, on the other hand, the loss of hydroxyl groups would decrease. The more
223 loss ratio of Ce-BC should be caused by the loss of hydroxyl groups on the adsorbent(Yu et al. 2017).

The XRD spectrum of BC and Ce-BC was described in Figure 5, it was observed that no obvious peak in BC XRD spectrum, indicating that the inorganic matter with lattice energy from BC was ignorable. However, the obvious peaks at 28.5, 33.1 and 47.4 were observed at Ce-BC peak, which corresponded to (1 1 1), (2 0 0) and (2 2 0) reflections of the cubic fluorite structure of CeO_2(Kouotou et al. 2021, Zhang et al. 2016a) (JCPDS: 034–0394), implying that Ce had been loaded onto the surface of BC.

3.2. The discussion of adsorption experiment

3.2.1. Effect of time

The effect of contact time on adsorption capacity was shown in Figure S1 of the SI. Both materials exhibited a typical initial rapid adsorption stage, followed by a slowing rate and gradual approach to adsorption equilibrium. However, Ce-BC demonstrated superior adsorption capacity and rate throughout the process compared to BC. The adsorption process was very rapid within the first 2 hours, with a sharp increase in adsorption capacity, then the rate slowed and essentially reached equilibrium after about 8 hours. The equilibrium adsorption capacity for Ce-BC was approximately 11 mg/g, while the capacity of BC was about 9 mg/g. Both the initial adsorption rate and final equilibrium capacity of BC were lower than those of Ce-BC. This is because phosphorus adsorption onto BC relies primarily on physical adsorption provided by its porous structure and weak electrostatic interactions with a small number of surface oxygen functional groups. In contrast, the high adsorption performance of Ce-BC is mainly attributed to specific chemical interactions between the loaded cerium species and phosphate ions. After the rapid initial stage, the adsorption rate slowed, likely due to the diffusion of phosphate ions into partially blocked pores or to deeper active sites within the cerium particles. The results indicate that the optimal adsorption time for both adsorbents is essentially 8 hours to achieve efficient and high-capacity phosphorus removal.

3.2.2. Effect of initial concentration

As shown in Figure S2 of the SI, the adsorption capacities of both BC and Ce-BC increased rapidly with increasing initial phosphorus concentration. When the initial concentration reached or exceeded 100 mg/L, the adsorption capacity gradually tended to plateau. This is because, at lower concentrations, phosphorus cannot occupy all the adsorption sites on BC or Ce-BC during the initial adsorption phase. In high phosphorus concentration environments, the concentration gradient would

provide more driving force to overcome the mass transfer resistance between the phosphate ions and BC or Ce-BC from liquid phase to solid phase, so that there were more adsorbates reaching to the surface of adsorbents and binding to adsorbent sites. And the driving force can enable phosphate ions to more effectively undergo ligand exchange with cerium active sites and form stable inner-sphere complexes thus demonstrating adsorption capacity and potential far exceeding that of BC. The obtained results showed that cerium modification successfully transformed the adsorption mechanism of biochar from one dominated by easily saturable physical and weak chemical interactions to one dominated by high-capacity, specific chemisorption.

3.2.3. Effect of adsorbent dosage

The dosage was significant in the adsorption process. As shown in Figure S3 of the SI, the adsorption capacities of BC and Ce-BC both decreased with the increase of adsorbent dosage. This was because that the adsorbent sites would contact with adsorbates and achieve saturation with a low dosage. However, with more dosage, there were more and more adsorption sites would fail to contact the adsorbates, leading to abundant unsaturated adsorption sites and further decreasing the adsorption capacity. In addition, the excess adsorbent dosage would induce the agglomeration between adsorbents(Song et al. 2017). However, it was observed that the removal rates were improved with the increased adsorbents, which was due to that the total surface area of the adsorbents increased with the more dosage, thus, there were more adsorption sites can bind the adsorbates. In addition, the removal ratios of BC and Ce-BC would keep constat with the limit dosage, which was because that the concentration gradient of the residual MB in solution was not enough to overcome the mass transfer resistance of the solution and the adsorbent surface and to bind with the empty adsorption site with limited concentration of adsorbates.

3.3 Adsorption isotherm

To further analyze the obtained adsorption data, a series of isotherm model were applied in this work. The Langmuir, Freundlich and Dubinin-Radushkevich (D-R) isotherm models were generally applied to simulate the results(Henninger et al. 2025, Rajahmundry et al. 2021, Singh and Kayal 2022, Young et al. 2021). The Langmuir and Freundlich models were described as below:

Langmuir isotherm model:

$$q_e = \frac{q_m K_L C_e}{1+K_L C_e} \quad (3)$$

Freundlich isotherm model:

$$q_e = K_F C_e^{\frac{1}{n}} \quad (4)$$

where q_e (mg/g) is the amount of uptake at equilibrium; C_e (mg/L) is the equilibrium concentration of the phosphorus; q_m (mg/g) is the maximum phosphorus uptake of the Langmuir isotherm; and K_F, K_L and n are constants related to adsorption.

The Dubinin-Radushkevich (D-R) model is states by the following equations:

$$q_e = q_m \exp(-K\varepsilon^2) \quad (5)$$

$$\varepsilon = \mathrm{RTln}(1 + \frac{1}{C_e}) \quad (6)$$

$$\mathrm{E} = \frac{1}{\sqrt{2K}} \quad (7)$$

where q_e (mg/g) is the amount of uptake at equilibrium; q_m (mg/g) is the maximum phosphorus uptake of the isotherm; ε is the Polanyi potential; T (K) is the absolute temperature; R is the gas constant (8.314 J/(mol•K)); and E (kJ/mol) is the free energy of sorption; if the value of E is below 8, the adsorption process is a physical process, while if the value of E is above 8, the adsorption process depends on a chemical process.

The adsorption isotherm models for BC and Ce-BC are shown in Figures 6 and S4 of the SI, and the model fitting parameters are listed in Table S2 of the SI. As to BC, the values of R^2 in D-R model were higher than those in other two models, indicating that the adsorption of P via BC was more suitable to D-R model. In addition, the increased values of q_m also indicated the higher temperature was favorable for the adsorption of P. Besides, from the parameters of other models, it was estimated from the value of K_L whether the isotherm is unfavorable ($K_L > 1$), linear ($K_L = 1$), favorable ($0 < K_L < 1$) or irreversible ($K_L = 1$), and it was observed the obtained K_L values were all from 0 to 1. As to Ce-BC, it was found that D-R model was best employed to fit the adsorption process with the highest values of R^2. And, the higher values of E (> 8) obtained from D-R model implied that the adsorption of Ce-BC for P depended on a chemical process. The increased q_m values, represent the represent the maximum adsorption capacity (from 24.67 to 26.22 mg/g) confirmed that higher temperatures can promote the adsorption process

3.4 Adsorption kinetic study

In this work, the pseudo-first-order, pseudo-second-order, the external and intraparticle diffusion models are used to fit the obtained adsorption data(Extross et al. 2022, Haddadi et al. 2022, Mahmud et al. 2022, Wasilewska et al. 2024), which were stated as below:

The pseudo-first-order equation:

$$q_t = q_e(1 - \exp(-k_1 \times t)) \quad (8)$$

The pseudo-second-order equation:

$$\frac{\mathrm{t}}{q_t} = \frac{1}{k_2 q_e^2} + \frac{t}{q_e} \quad (9)$$

$$\mathrm{h} = k_2 (q_e)^2 \quad (10)$$

The external diffusion equation:

$$\ln C_t = ln C_0 - k_{ext} t \quad (11)$$

The intraparticle diffusion equation:

$$q_t = k_{p,i} \times t^{0.5} \quad (12)$$

where q_t (mg/g) is the amount of adsorbate absorbed per gram adsorbent at time t; *qe* (mg/g) is the amount of adsorbate adsorbed per unit mass adsorbent at equilibrium; k_1 (min^{-1}) is the rate constant of pseudo-first-order adsorption; k_2 (min^{-1}) is the rate constant of pseudo-first-order adsorption; and *h* (mg/(g•min)) is the initial reaction rate. k_{ext} (1/min) is the constant of external diffusion; C_t (mg/L) is the concentration of the adsorbate at time t, C_0 (mg/L) is the initial concentration. q_t (mg/g) is the adsorption capacity at time *t*, and $k_{p,i}$ (mg/(g•min)) is the constant of intraparticle diffusion in the *i* phase.

The kinetic models simulated for phosphorus were shown in Figures of S5 and S6 of the SI. The corresponded parameters were described in Table S3 of the SI. As to BC, the higher value of R^2 (0.994) meant that the pseudo-first-order model was more suitable to describe the P adsorption kinetic process by the BC. However, it was more propitious to the pseudo-second-order model (R^2 = 0.996) by the Ce-BC, implying that the adsorption process of phosphorus via the Ce-BC was a chemical reaction due to the pseudo-second-order kinetic model was established via a hypothesis of chemical adsorption based on electron transfer. In addition, the external and intraparticle diffusion models were used to fit the

obtained data from a micro perspective. In terms of external diffusion model, the linear relationship between ln (C_t) and t indicated that the external diffusion was crucial during the initial adsorption process. Besides, the intraparticle diffusion model can be divided into two stages, where the first linear relationship of q_t versus $t^{0.5}$ can not pass through the origin, implying that the adsorption of phosphorus by BC and Ce-BC were the only rate-controlling step.

3.5 Thermodynamic study

The simulated thermodynamic data for the P adsorption capacities by the BC and Ce-BC at different temperatures was illustrated in Figure S7 of the SI, and calculated parameters were listed in Table S4 of the SI. It can be found that the negative value of ΔG^0 reduced with the higher temperature from the Table S4 of the SI, implying that the adsorption of P by the abovementioned adsorbents was spontaneous and completed more easily in the high temperature condition (Fu et al. 2015). The result also was consistent with the conclusion induced from the above isotherm model simulation. Furthermore, the positive values of ΔH^0 and ΔS^0 indicated that the adsorption process of P by the BC and Ce-BC was all endothermic, and demonstrated the enough degree of freedom at the solid-liquid interface can improve the adsorption efficiency of the adsorbates (Bedin et al. 2016).

3.6 Effect of pH

The role of pH in the adsorption of phosphorus was important due to P owned various species in different pH solutions shown in Figure S8 of the SI. In addition, it was observed that the phosphorus capture of Ce-BC achieved the highest value at initial pH 5 from the Figure S10 of the SI. Combined the values of Zeta (Figure S9 of the SI), the surface charge of Ce-BC was positive at pH < 6.39, where the main species of phosphorus were H_3PO_4 and $H_2PO_4^-$, leading to a stronger electrostatic attraction between negative surface charge and $H_2PO_4^-$. Besides, the week adsorption capacity of Ce-BC at pH ranging from 2 to 5 may be due to the presence of neutral specie (H_3PO_4) which would weaken the electrostatic attraction. During the pH > 6, a positively charged surface would be formed on the adsorbent surface, which would inhibit the phosphorus uptake due to the enhancement of electrostatic repulsion between adsorbent and negative species (HPO_4^{2-} and PO_4^{3-}). The phosphorus adsorption process via BC was approximate to that of Ce-BC, but the similar pH_{zpc} and the more adsorption capacity of Ce-BC both implied that the phosphorus uptake by Ce-BC was not completely dominated

by electrostatic attraction, also include the binding sites mainly provided by -OH groups in Ce-BC(Zhang et al. 2016b).

3.7 Recyclability and regeneration

To evaluate the regeneration performance of Ce-BC, the desorption efficiency and recycling ratio of Ce-BC was conducted and presented in Figure S11 of the SI. After eight adsorption–desorption cycle, the recycling of Ce-BC still held above 80%, and the eight repeated washing of sodium hydroxide make the adsorption capacity of Ce-BC kept about 9 mg/g, implying that the Ce-BC had great engineering-application potential in water treatment under the elution of sodium hydroxide.

4. Conclusion

This study successfully prepared cerium-modified bamboo-based biochar composite (Ce-BC) via a hydrothermal method and systematically investigated its adsorption performance and mechanism for phosphorus. Characterization results confirmed that cerium was firmly anchored onto the biochar surface in the form of nanoparticles. FTIR analysis showed an increase in characteristic peaks for the modified biochar compared to the unmodified version, indicating a more diverse array of functional groups and significantly enhanced chemisorption contributions. Adsorption experiments confirmed that compared to pristine biochar, Ce-BC increase in the adsorption rate constant and maintained excellent performance under various environmental conditions, demonstrating significantly improved environmental adaptability. Among the factors, contact time was most critical for the adsorption performance of the modified biochar, with optimal adsorption observed around 8 hours, an initial concentration ≥100 mg/L, and an adsorbent dosage of 0.5 g. Excessive adsorbent dosage and initial concentration led to decreased adsorption efficiency. Kinetic and isotherm studies further demonstrated that the adsorption process followed the pseudo-second-order kinetic model and was dominated by monolayer chemisorption. This study verifies that cerium modification fundamentally shifts the adsorption mechanism of biochar from physical adsorption dominance to chemisorption dominance, providing an important theoretical basis and practical reference for designing and developing efficient phosphorus recovery materials.

Author Contributions

Lang Wang: Writing–original draft, Formal analysis, Data curation, Conceptualization. Zhiyi Sun:

Methodology, Investigation, Data curation. Haitao Sha: Writing – review & editing, Investigation, Data curation, Conceptualization. Hui Wang: Writing – original draft, Data curation, Conceptualization.

Funding

This work was financially supported by the National Natural Science Foundation of China (No. 22406013), Changzhou Science and Technology Program (NO. CJ20250084) and the Natural Science Foundation of Jiangsu Province (NO. BK20240338 and NO. BK20240339).

Data Availability

The datasets used and analyzed during the current study are available from the corresponding author on reasonable request

Declarations

Ethical Approval

Not applicable. This study did not involve human participants or animal experiments.

Competing Interests

The authors declare no competing interests.

Reference

Abdo, H.S., Alnaser, I.A., Seikh, A.H., Mohammed, J.A., Ragab, S.A., Fouly, A. and Wu, Q. (2023) Ecofriendly Biochar as a Low-Cost Solid Lubricating Filler for LDPE Sustainable Biocomposites: Thermal, Mechanical, and Tribological Characterization. *International Journal of Polymer Science,* 2023, 1-13. https://doi.org/10.1155/2023/2445472

Abdullah, F.H., Bakar, N. and Bakar, M.A. (2022) Current advancements on the fabrication, modification, and industrial application of zinc oxide as photocatalyst in the removal of organic and inorganic contaminants in aquatic systems. *J Hazard Mater,* 424, 127416. https://doi.org/10.1016/j.jhazmat.2021.127416

Amalina, F., Razak, A.S.A., Krishnan, S., Zularisam, A.W. and Nasrullah, M. (2022) A comprehensive assessment of the method for producing biochar, its characterization, stability, and potential applications in regenerative economic sustainability – A review. *Cleaner Materials,* 3. https://doi.org/10.1016/j.clema.2022.100045

An, N.N., Duong, N.S., Hung, H.M., Xuan, V.T. and Thao, T. (2024) Characteristics and Methylene Blue Adsorption Capacity of Pyrochar Derived from Lemongrass Residue. *VNU Journal of Science: Natural Sciences and Technology,* 40. https://doi.org/10.25073/2588-1140/vnunst.5271

Ashiq, A., Sarkar, B., Adassooriya, N., Walpita, J., Rajapaksha, A.U., Ok, Y.S. and Vithanage, M. (2019) Sorption process of municipal solid waste biochar-montmorillonite composite for ciprofloxacin removal in aqueous media. *Chemosphere,* 236. https://doi.org/10.1016/j.chemosphere.2019.124384

Bedin, K.C., Martins, A.C., Cazetta, A.L., Pezoti, O. and Almeida, V.C. (2016) KOH-activated carbon prepared from sucrose spherical carbon: Adsorption equilibrium, kinetic and thermodynamic studies for Methylene

Blue removal. *Chem. Eng. J.,* 286, 476-484. https://doi.org/10.1016/j.cej.2015.10.099

Bhardwaj, K. and Singh, A.K. (2023) Bio-waste and natural resource mediated eco-friendly synthesis of zinc oxide nanoparticles and their photocatalytic application against dyes contaminated water. *Chemical Engineering Journal Advances,* 16. https://doi.org/10.1016/j.ceja.2023.100536

Brooker, M.R., Longnecker, K., Kujawinski, E.B., Evert, M.H. and Mouser, P.J. (2018) Discrete Organic Phosphorus Signatures are Evident in Pollutant Sources within a Lake Erie Tributary. *Environ Sci Technol,* 52, 6771-6779. https://doi.org/10.1021/acs.est.7b05703

Durairaj, K.R., Kannan, M., Jayakumar, R., Dharmaraj, D., Sundaram, T. and Shubing, Z. (2024) Toxic effects of organophosphate pesticide monocrotophos in aquatic organisms: A review of challenges, regulations and future perspectives. *Environmental Research,* 244, 117947-. https://doi.org/10.1016/j.Envres.2023.117947

Extross, A., Waknis, A., Tagad, C., Gedam, V.V. and Pathak, P.D. (2022) Adsorption of congo red using carbon from leaves and stem of water hyacinth: equilibrium, kinetics, thermodynamic studies. *International Journal of Environmental Science and Technology,* 20, 1607-1644. https://doi.org/10.1007/s13762-022-03938-x

Fionah, A., Oluk, I., Brady, L., Byrne, D.M. and Escobar, I.C. (2024) Performance and Environmental Assessment of Biochar-Based Membranes Synthesized from Traditional and Eco-Friendly Solvents. *Membranes,* 14. https://doi.org/10.3390/membranes14070153

Fu, J.W., Chen, Z.H., Wang, M.H., Liu, S.J., Zhang, J.H., Zhang, J.N., Han, R.P. and Xu, Q. (2015) Adsorption of methylene blue by a high-efficiency adsorbent (polydopamine microspheres): Kinetics, isotherm, thermodynamics and mechanism analysis. *Chem. Eng. J.,* 259, 53-61. https://doi.org/10.1016/j.cej.2014.07.101

Gray, H.E., Powell, T., Choi, S., Smith, D.S. and Parker, W.J. (2020) Organic phosphorus removal using an integrated advanced oxidation-ultrafiltration process. *Water Res,* 182, 115968. https://doi.org/10.1016/j.watres.2020.115968

Haddadi, E., Gujar, J.G. and Sonawane, S.S. (2022) Kinetics and isotherm studies for the adsorption of boron from water using titanium dioxide. *The Canadian Journal of Chemical Engineering,* 101, 1335-1344. https://doi.org/10.1002/cjce.24429

Henninger, M., Postweiler, P., Engelpracht, M., Galvanin, F. and Bardow, A. (2025) Model-based design of experiments for adsorption isotherms. *Adsorption,* 31. https://doi.org/10.1007/s10450-025-00653-0

Imran, A. and Ahmed, S. (2025) Innovative approaches to adsorptive detoxification of pesticides in aquatic environments: a comprehensive review. *International Journal of Environmental Science and Technology,* 22, 8377-8404. https://doi.org/10.1007/s13762-025-06350-3

Janarthanan, B., Thirunavukkarasu, C., Maruthamuthu, S., Manthrammel, M.A., Shkir, M., AlFaify, S., Selvakumar, M., Reddy, V.R.M. and Park, C. (2021) Basic deposition methods of thin films**. *Journal of Molecular Structure,* 1241. https://doi.org/10.1016/j.molstruc.2021.130606

Jatoi, A.S., Hashmi, Z., Adriyani, R., Yuniarto, A., Mazari, S.A., Akhter, F. and Mubarak, N.M. (2021) Recent trends and future challenges of pesticide removal techniques – A comprehensive review. *Journal of Environmental Chemical Engineering,* 9. https://doi.org/10.1016/j.jece.2021.105571

Khayyam Nekouei, R., Hajian-Foroushani, M., Maroufi, S., S. Mofarah, S.S., Akhter, R., Biswal, S., Bustamante, H. and Sahajwalla, V. (2024) Microwave-assisted transforming of biosolids into engineered activated carbon employed for adsorption from wastewater. *Journal of Cleaner Production,* 467.

https://doi.org/10.1016/j.jclepro.2024.142941
Komnitsas, K., Zaharaki, D., Bartzas, G. and Alevizos, G. (2017) Adsorption of Scandium and Neodymium on Biochar Derived after Low-Temperature Pyrolysis of Sawdust. *Minerals,* 7. https://doi.org/10.3390/min7100200
Kouotou, D., Ghalit, M., Ndi, J.N., Martinez, L.M.P., Ouahabi, M.E., Ketcha, J.M. and Gharibi, E.K. (2021) Removal of metallic trace elements (Pb(2+), Cd(2+), Cu(2+), and Ni(2+)) from aqueous solution by adsorption onto cerium oxide modified activated carbon. *Environ Monit Assess,* 193, 467. https://doi.org/10.1007/s10661-021-09267-9
Ksapabutr, B., Gulari, E. and Wongkasemjit, S. (2004) One-pot synthesis and characterization of novel sodium tris(glycozirconate) and cerium glycolate precursors and their pyrolysis. *Materials Chemistry and Physics,* 83, 34-42. https://doi.org/10.1016/j.matchemphys.2003.08.016
Kumar, P., Singhania, R.R., Sumathi, Y., Kurrey, N.K., Chen, C.-W., Patel, A.K. and Dong, C.-D. (2024) Investigating innovative techniques for biochar modification to enhance the removal of heavy metals from aqueous environments: a comprehensive review. *Clean Technologies and Environmental Policy,* 27, 3271-3293. https://doi.org/10.1007/s10098-024-02962-4
Li, M., Li, L., Sun, Y., Ma, H., Zhang, H. and Li, F. (2023) Facile synthesis of dual-hydrolase encapsulated magnetic ZIF-8 composite for efficient removal of multi-pesticides induced pollution in water. *Chemosphere,* 314, 137673. https://doi.org/10.1016/j.chemosphere.2022.137673
Li, R., Li, Q., Gao, S. and Shang, J.K. (2012) Exceptional arsenic adsorption performance of hydrous cerium oxide nanoparticles: Part A. Adsorption capacity and mechanism. *Chemical Engineering Journal,* 185-186, 127-135. https://doi.org/10.1016/j.cej.2012.01.061
Liang, L., Xi, F., Tan, W., Meng, X., Hu, B. and Wang, X. (2021) Review of organic and inorganic pollutants removal by biochar and biochar-based composites. *Biochar,* 3, 255-281. https://doi.org/10.1007/s42773-021-00101-6
Lyu, H., Zhang, Q. and Shen, B. (2020) Application of biochar and its composites in catalysis. *Chemosphere,* 240, 124842. https://doi.org/10.1016/j.chemosphere.2019.124842
Mahmud, M., Sahadat Hossain, M., Bin Mobarak, M., Sultana, S., Sharmin, S. and Ahmed, S. (2022) Co-precipitation synthesis of non-cytotoxic and magnetic cobalt ferrite nanoparticles for purging heavy metal from the aqueous medium: Pb(II) adsorption isotherms and kinetics study. *Chemistry and Ecology,* 38, 544-563. https://doi.org/10.1080/02757540.2022.2093351
Mankomal and Kaur, H. (2022) Synergistic effect of biochar impregnated with ZnO nano-flowers for effective removal of organic pollutants from wastewater. *Applied Surface Science Advances,* 12. https://doi.org/10.1016/j.apsadv.2022.100339
Marien, C.B.D., Le Pivert, M., Azaïs, A., M'Bra, I.C., Drogui, P., Dirany, A. and Robert, D. (2019) Kinetics and mechanism of Paraquat's degradation: UV-C photolysis vs UV-C photocatalysis with TiO2/SiC foams. *Journal of Hazardous Materials,* 370, 164-171. https://doi.org/10.1016/j.jhazmat.2018.06.009
Mel'gunov, M.S. (2022) Application of the simple Bayesian classifier for the N2 (77 K) adsorption/desorption hysteresis loop recognition. *Adsorption,* 29, 199-208. https://doi.org/10.1007/s10450-022-00369-5
Paerl, H.W., Otten, T.G. and Kudela, R. (2018) Mitigating the Expansion of Harmful Algal Blooms Across the Freshwater-to-Marine Continuum. *Environ Sci Technol,* 52, 5519-5529. https://doi.org/10.1021/acs.est.7b05950
Pandiarajan, S., Sankararajan, V., Dinesh kumar, N. and Swaminathan, M. (2025) Characterization and

performance of activated biochar-doped zinc oxide in domestic wastewater treatment. *Journal of the Indian Chemical Society,* 102. https://doi.org/10.1016/j.jics.2025.102010

Pasieczna-Patkowska, S., Cichy, M. and Flieger, J. (2025) Application of Fourier Transform Infrared (FTIR) Spectroscopy in Characterization of Green Synthesized Nanoparticles. *Molecules,* 30. https://doi.org/10.3390/molecules30030684

Ponnuchamy, M., Kapoor, A., Senthil Kumar, P., Vo, D.-V.N., Balakrishnan, A., Mariam Jacob, M. and Sivaraman, P. (2021) Sustainable adsorbents for the removal of pesticides from water: a review. *Environmental Chemistry Letters,* 19, 2425-2463. https://doi.org/10.1007/s10311-021-01183-1

Rajahmundry, G.K., Garlapati, C., Kumar, P.S., Alwi, R.S. and Vo, D.N. (2021) Statistical analysis of adsorption isotherm models and its appropriate selection. *Chemosphere,* 276, 130176. https://doi.org/10.1016/j.chemosphere.2021.130176

Ryu, H.D., Han, H., Park, J.H. and Kim, Y.S. (2022) New insights into the occurrence and removal of 36 pesticides in pesticide wastewater treatment plants in Korea. *Chemosphere,* 309, 136717. https://doi.org/10.1016/j.chemosphere.2022.136717

Sathishkumar, K., Li, Y. and Sanganyado, E. (2020) Electrochemical behavior of biochar and its effects on microbial nitrate reduction: Role of extracellular polymeric substances in extracellular electron transfer. *Chemical Engineering Journal,* 395. https://doi.org/10.1016/j.cej.2020.125077

Sha, H., Su, X., Chen, X., Wang, L., Wang, S., Ke, Y. and Zhou, P. (2024) Effect of dissolution for black carbon on the adsorption capacity for methylene blue: Equilibrium, kinetics and thermodynamics. *Journal of Dispersion Science and Technology*, 1-11. https://doi.org/10.1080/01932691.2024.2378184

Sharma, A., Kumar, V., Shahzad, B., Tanveer, M., Sidhu, G.P.S., Handa, N., Kohli, S.K., Yadav, P., Bali, A.S., Parihar, R.D., Dar, O.I., Singh, K., Jasrotia, S., Bakshi, P., Ramakrishnan, M., Kumar, S., Bhardwaj, R. and Thukral, A.K. (2019) Worldwide pesticide usage and its impacts on ecosystem. *SN Applied Sciences,* 1. https://doi.org/10.1007/s42452-019-1485-1

Sing, K.S.W. and Williams, R.T. (2004) Physisorption Hysteresis Loops and the Characterization of Nanoporous Materials. *Adsorption Science & Technology,* 22, 773-782. https://doi.org/10.1260/0263617053499032

Singh, A. and Kayal, S. (2022) Investigation of methane adsorption onto metal–organic frameworks under subcritical condition employing adsorption isotherm models. *Bulletin of Materials Science,* 45. https://doi.org/10.1007/s12034-022-02685-6

Song, X., Li, L., Geng, Z., Zhou, L. and Ji, L. (2017) Effective and selective adsorption of As(III) via imprinted magnetic Fe 3 O 4 /HTCC composite nanoparticles. *Journal of Environmental Chemical Engineering,* 5, 16-25. https://doi.org/10.1016/j.jece.2016.11.016

Tony, M.A. and Mansour, S.A. (2019) Microwave-assisted catalytic oxidation of methomyl pesticide by Cu/Cu2O/CuO hybrid nanoparticles as a Fenton-like source. *International Journal of Environmental Science and Technology,* 17, 161-174. https://doi.org/10.1007/s13762-019-02436-x

Wasilewska, M., Derylo-Marczewska, A. and Marczewski, A.W. (2024) Equilibrium and Kinetic Studies on Adsorption of Neutral and Ionic Species of Organic Adsorbates from Aqueous Solutions on Activated Carbon. *Molecules,* 29. https://doi.org/10.3390/molecules29133032

Young, J., García-Díez, E., Garcia, S. and van der Spek, M. (2021) The impact of binary water–CO2 isotherm models on the optimal performance of sorbent-based direct air capture processes. *Energy & Environmental Science,* 14, 5377-5394. https://doi.org/10.1039/d1ee01272j

Yu, Y., Zhang, C., Yang, L. and Paul Chen, J. (2017) Cerium oxide modified activated carbon as an efficient and

effective adsorbent for rapid uptake of arsenate and arsenite: Material development and study of performance and mechanisms. *Chemical Engineering Journal,* 315, 630-638. https://doi.org/10.1016/j.cej.2016.09.068

Zhang, B., Xu, L., Zhao, Z., Peng, S., Yu, C., Zhang, X., Zong, Y. and Wu, D. (2022) Enhanced phosphate removal by nano-lanthanum hydroxide embedded silica aerogel composites: Superior performance and insights into specific adsorption mechanism. *Separation and Purification Technology,* 285. https://doi.org/10.1016/j.seppur.2021.120365

Zhang, L., Zhu, T., Liu, X. and Zhang, W. (2016a) Simultaneous oxidation and adsorption of As(III) from water by cerium modified chitosan ultrafine nanobiosorbent. *Journal of Hazardous Materials,* 308, 1-10. https://doi.org/10.1016/j.jhazmat.2016.01.015

Zhang, Y., Pan, B., Shan, C. and Gao, X. (2016b) Enhanced Phosphate Removal by Nanosized Hydrated La(III) Oxide Confined in Cross-linked Polystyrene Networks. *Environ Sci Technol,* 50, 1447-1454. https://doi.org/10.1021/acs.est.5b04630

Zhao, C., Ma, J., Li, Z., Xia, H., Liu, H. and Yang, Y. (2020) Highly enhanced adsorption performance of tetracycline antibiotics on KOH-activated biochar derived from reed plants. *RSC Advances,* 10, 5066-5076. https://doi.org/10.1039/c9ra09208k

Zhao, T., Hu, K., Li, J., Zhu, Y., Liu, A., Yao, K. and Liu, S. (2021) Current insights into the microbial degradation for pyrethroids: strain safety, biochemical pathway, and genetic engineering. *Chemosphere,* 279, 130542. https://doi.org/10.1016/j.chemosphere.2021.130542

Zhou, X., Zhu, Y., Niu, Q., Zeng, G., Lai, C., Liu, S., Huang, D., Qin, L., Liu, X., Li, B., Yi, H., Fu, Y., Li, L., Zhang, M., Zhou, C. and Liu, J. (2021) New notion of biochar: A review on the mechanism of biochar applications in advannced oxidation processes. *Chemical Engineering Journal,* 416. https://doi.org/10.1016/j.cej.2021.129027

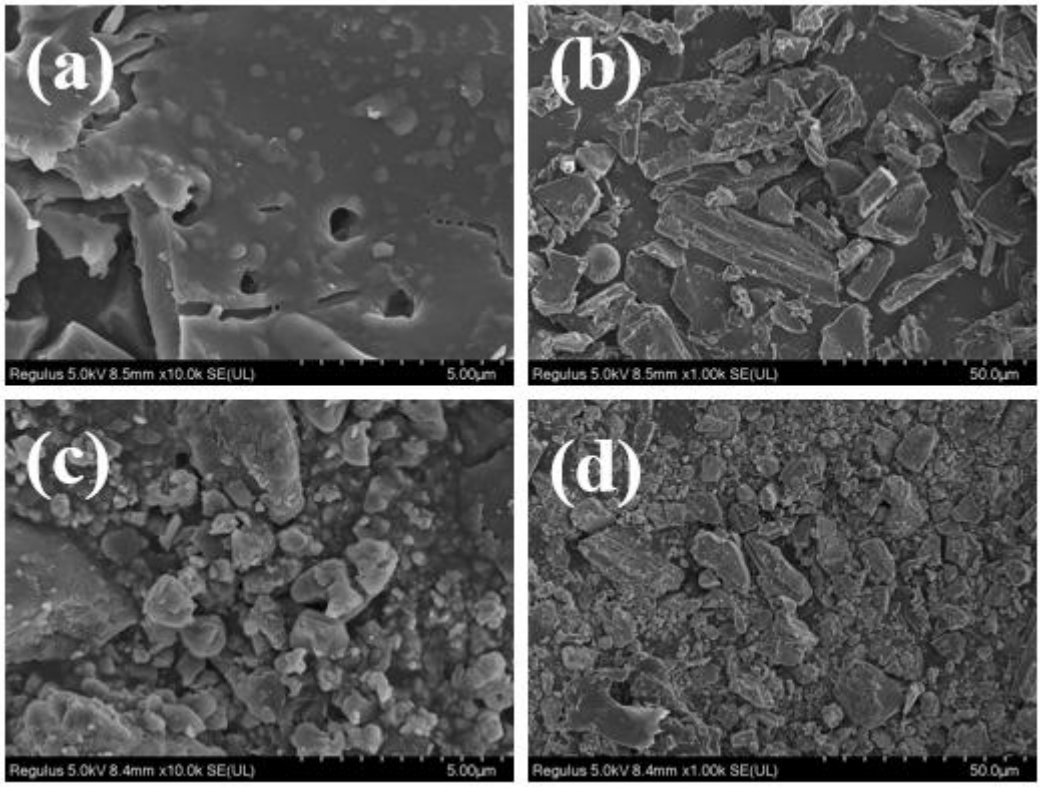


Figure 1. SEM images of BC-5μm (a), BC-50μm (b), Ce-BC-5μm (c) and Ce-BC-50μm(d).

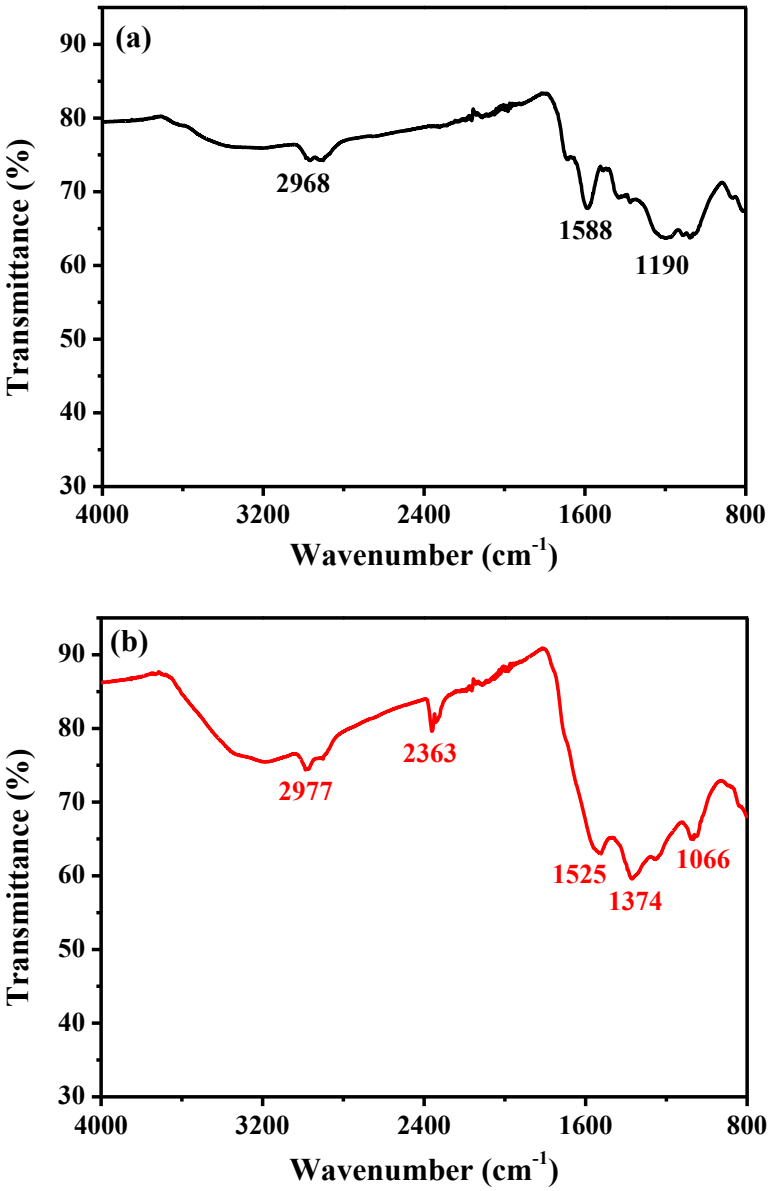


Figure 2. FTIR spectra of BC (a) and Ce-BC (b).

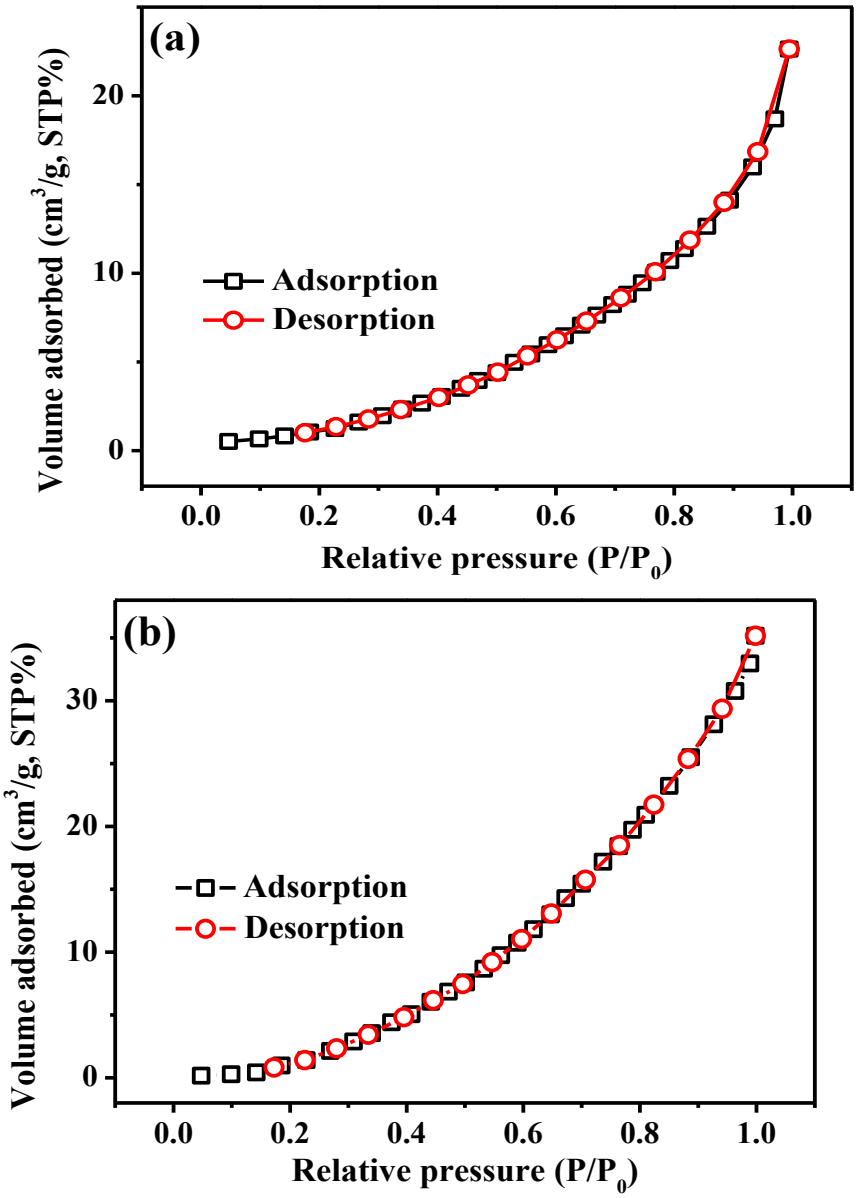


Figure 3. N_2 adsorption-desorption isotherms of BC (a) and Ce-BC (b)

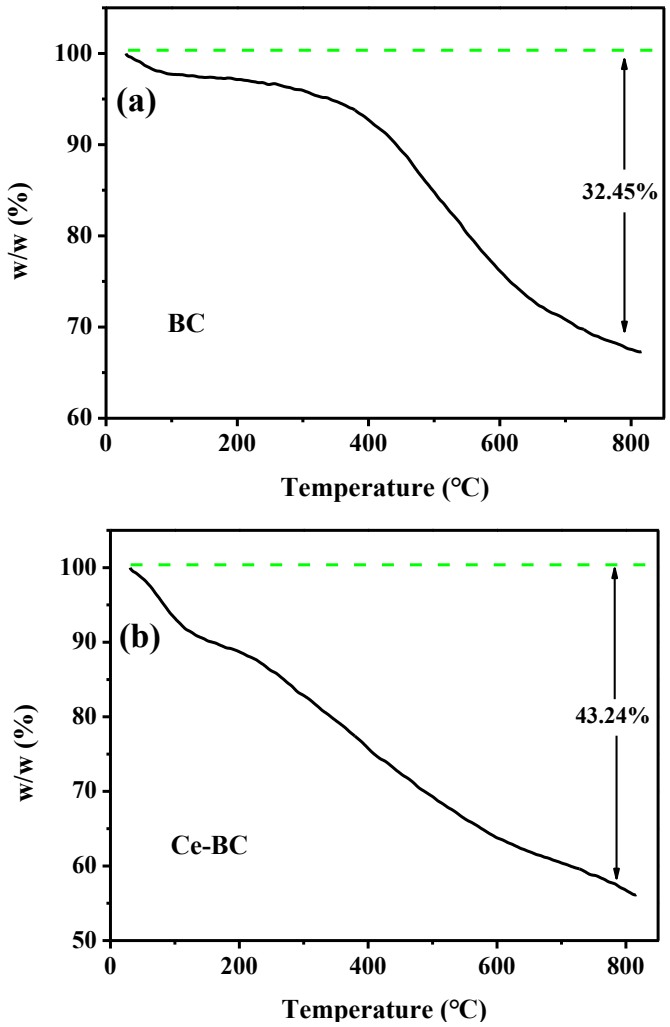


Figure 4. TG curves of BC (a) and Ce-BC (b).

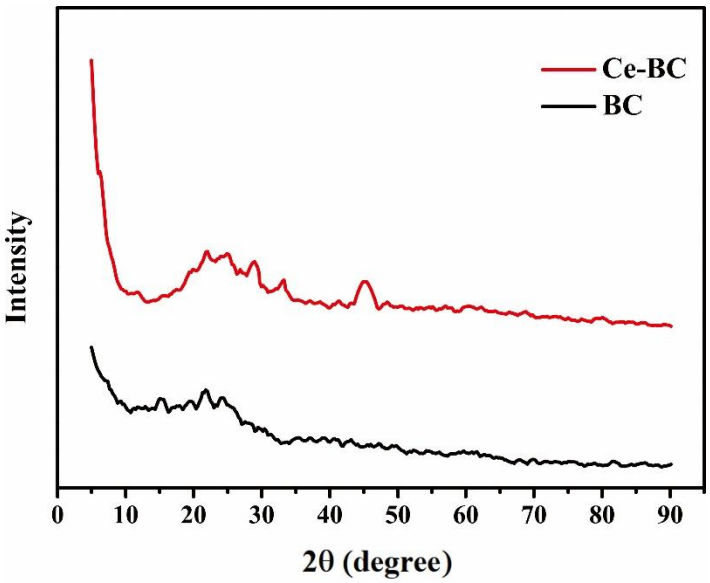
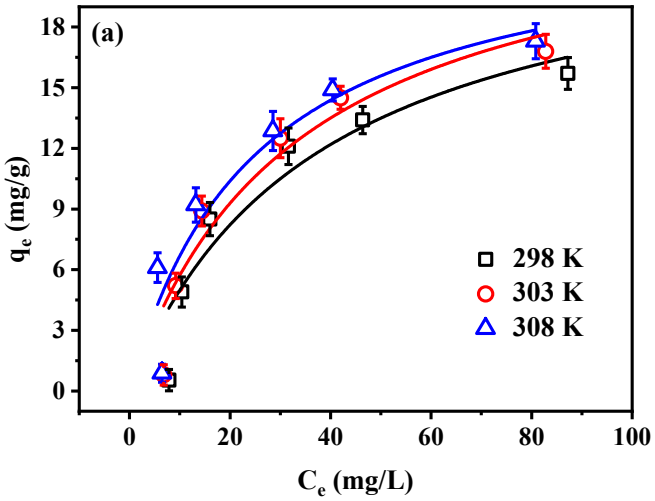
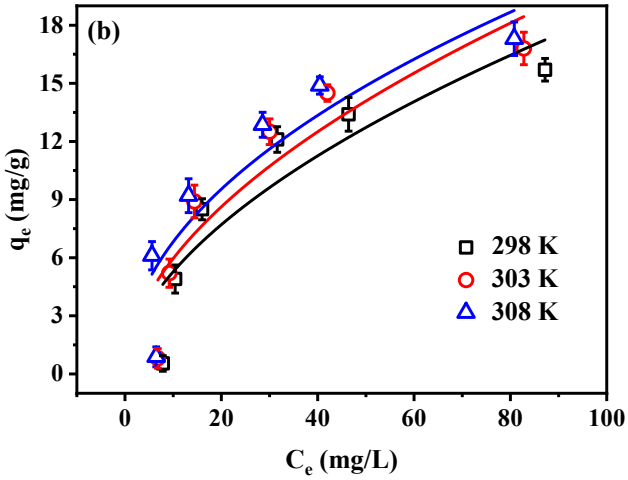


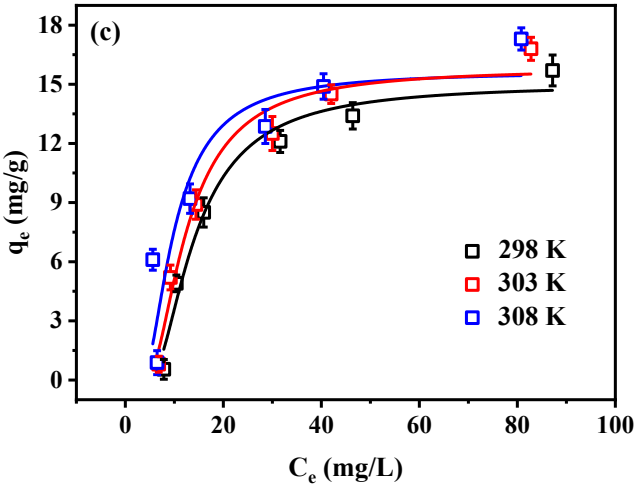
Figure. 5 XRD spectra of BC and Ce-BC.



686



687



688

689 **Figure 6.** Isotherm models for P adsorption by BC under different temperatures at the optimal adsorption condition

690 (a) Langmuir isotherm model; (b) Freundlich isotherm model; (c) D-R isotherm model.

691

Supplementary Files

This is a list of supplementary files associated with this preprint. Click to download.

- supportinginformation.docx